Construction and Building Materials 530 (2026) 146661

Contents lists available at ScienceDirect

Construction and Building Materials

journal homepage: www.elsevier.com/locate/conbuildmat

Thermal and hygrothermal performance of Arundo donax shive–lime composites for sustainable building insulation

Mebratu Tufa *, Zoltán Pásztory

University of Sopron, Faculty of Wood Engineering and Creative Industry, Hungary

ARTICLE INFO

Keywords:
Arundo donax
Lime composites
Bio-based insulation
Thermal conductivity
Temperature dependence
Sustainable construction materials

ABSTRACT

The construction sector is under increasing pressure to reduce energy consumption and carbon emissions, driving the development of bio-based, low-impact insulation materials. Lime composites incorporating plant aggregates are promising alternatives to conventional insulation; however, the potential of Arundo donax as a bio-aggregate remains underexplored. This study evaluates the physical, thermal, and hygrothermal performance of Arundo donax shive–lime composites produced with binder-to-shive mass ratios of 1:1, 1.5:1, and 2:1. Composite panels were prepared using CL90 slaked lime and cured under controlled conditions. Apparent density, water absorption, and thermal conductivity were measured after 28 days, including temperature-dependent thermal conductivity over the range −10–50 °C. Microstructural and chemical characterisation was performed using SEM, EDX, and FTIR. Dry apparent density increased from 302 to 445 kg·m^{-3} with increasing binder content due to matrix densification and carbonation. Thermal conductivity rose linearly with density (0.072–0.092 W·m^{-1}·K^{-1}), confirming density as the dominant parameter governing heat transfer. Thermal conductivity also increased with temperature for all formulations, while temperature sensitivity decreased with increasing binder content, indicating enhanced thermal stability. Water absorption decreased markedly as binder content increased. SEM, EDX, and FTIR analyses confirmed effective lime coating of the shives, partial pore filling, and the formation of calcium carbonate, supporting the observed physical and thermal trends. Overall, Arundo donax–lime composites exhibit performance comparable to hemp–lime and other reed-based materials. The 1.5:1 binder-to-shive ratio provides the most balanced combination of low density, insulation performance, moisture resistance, and thermal stability, highlighting Arundo donax as a viable bio-aggregate for sustainable building insulation.

1. Introduction

The construction sector is among the largest contributors to global energy consumption and greenhouse gas emissions, with a substantial share attributed to the heating and cooling of buildings [1,2]. Enhancing the thermal performance of building envelopes is therefore a critical strategy for reducing operational energy demand. Conventional insulation materials, including expanded polystyrene, polyurethane foams, and mineral wool, are widely used for this purpose; however, their production is associated with high embodied energy, limited recyclability, and significant environmental impacts [3,4]. These drawbacks have motivated growing interest in sustainable, low-carbon alternatives.

Bio-based insulation materials derived from agricultural residues or rapidly renewable plant resources have emerged as promising substitutes [5]. Plant-based aggregates such as hemp shiv, flax, and straw have been extensively investigated in combination with lime binders to produce lightweight composites commonly referred to as plant-based concretes. These materials are characterized by low density and favorable thermal insulation properties, largely associated with their highly porous internal structure, while also contributing to carbon sequestration through the carbonation of lime during service life [6,7]. Lime is especially suitable as a binder due to its chemical compatibility with organic fibers, vapor permeability, and long-term durability [8,9].

From a material perspective, the performance of plant-based lime composites is strongly governed by density and its associated internal structure, which together control both thermal behavior and moisture interaction. Studies highlights that the thermal efficiency of bio-aggregated composites is fundamentally dictated by their internal architecture, specifically the multi-scale porosity of the vegetable particles. Research using advanced diagnostic techniques, such as thermal methods for assessing pore size distribution, has shown that internal pore geometry and connectivity are key factors controlling effective

* Corresponding author.
E-mail address: mebratu.tufa@uni-sopron.hu (M. Tufa).

https://doi.org/10.1016/j.conbuildmat.2026.146661
Received 13 February 2026; Received in revised form 7 April 2026; Accepted 7 May 2026
Available online 12 May 2026

thermal conductivity. In high-performance insulation materials, pore morphology including shape and orientation greatly influences heat resistance while the spatial arrangement of these voids ultimately determines the matrix's overall thermophysical properties [10–12]. This porosity is inherently reflected in bulk density and plays a key role in defining the balance between insulating capacity and material compactness. In this context, the relationship between density and thermal conductivity is widely recognized as a primary descriptor of heat transfer in bio-based composites.

Arundo donax L., commonly known as giant reed, is a perennial grass species widely distributed in Mediterranean and subtropical regions, where it is often considered invasive. The plant exhibits rapid growth, high annual biomass yield, and a naturally fibrous and porous internal structure [13,14]. Although Arundo donax has been explored for applications such as bioenergy production, pulp, and paper manufacturing, its potential use as an aggregate in bio-based insulation materials remains largely underexplored.

Recent investigations on Arundo donax–based composites confirm that their insulation performance is closely linked to density and internal structure. For example, Cintura et al. (2023) reported a thermal conductivity of approximately 0.128 $W{\cdot}m^{-1}{\cdot}K^{-1}$) together with significant moisture buffering capacity, reflecting the influence of a heterogeneous and interconnected pore network [15]. Similarly, the review by Leone et al. (2025) indicates that variations in particle size, morphology, and processing conditions directly affect density and internal structure, thereby influencing both thermal performance and moisture-related properties [16]. These findings emphasize that controlling material formulation is essential to achieving balanced performance. Other studies on hemp-lime and straw-lime composites report thermal conductivity values typically ranging from 0.06 to 0.12 W. $m^{-1}{\cdot}K^{-1}$, strongly influenced by material density, aggregate–binder ratio, and compaction level [6,17–19]. Density plays a central role in determining thermal performance, as higher binder content generally increases density and, consequently, thermal conductivity. For example, Walker and Pavía [20] demonstrated that increasing lime content in hemp-lime composites led to an increase in thermal conductivity from approximately 0.08–0.12 $W{\cdot}m^{-1}{\cdot}K^{-1}$

This density–thermal conductivity relationship is fundamentally associated with changes in internal structure, where increasing binder content promotes matrix continuity, reduces void fraction, and enhances solid-phase heat transfer. Similar trends have been reported in bio-based systems confirming that density can be used as a practical macroscopic parameter to describe heat transfer behavior [21], [22]. In addition, the hygroscopic nature of plant aggregates allows bio-based composites to absorb and release moisture, influencing heat transfer behavior. Lime-based binders contribute to moisture buffering capacity, enabling indoor humidity regulation, which is considered an additional functional advantage of bio-based materials [23,24].

In lime-based systems, binder content also governs microstructural development through hydration and carbonation processes. During curing, lime reacts with atmospheric CO_2 to form calcium carbonate, leading to progressive matrix densification and improved particle–-binder bonding. Pham (2014) showed that this transformation can modify internal structure and thermal properties over time [25]. Similarly, Hachem et al. (2023) reported that the incorporation of Arundo donax in cementitious matrices affects porosity and matrix continuity, while secondary reactions contribute to structural refinement. These processes highlight the role of binder proportion not only in determining density but also in shaping the final microstructure of the composite [26]. Nevertheless, mixtures optimized for thermal insulation often exhibit reduced mechanical performance, highlighting the need for balanced material design.

Despite the growing body of literature on hemp-based and straw-based lime composites, experimental data on Arundo donax–lime composites remain scarce. Given its widespread availability, low cost, and favorable morphological characteristics, Arundo donax represents a potentially competitive alternative in regions where traditional plant aggregates are limited or economically unviable. Furthermore, existing studies on Arundo donax–based materials often consider isolated properties or alternative binder systems, with limited experimental data addressing the combined influence of binder content, density, and temperature on the thermal performance of lime-based composites.

Despite increasing research on hemp- and straw-based composites, experimental data on Arundo donax–lime systems remain limited, particularly regarding the combined influence of binder content, density, and temperature on thermal performance. Furthermore, few studies systematically link macroscopic thermophysical properties to microstructural characteristics in such systems. This study addresses these gaps by experimentally evaluating the physical, thermal, and hygrothermal performance of Arundo donax shive–lime composites with varying binder-to-shive ratios. Particular emphasis is placed on the relationship between density and thermal conductivity, as well as the influence of temperature and binder content on thermal behavior, supported by microstructural and chemical characterization.

2. Materials and methods

2.1. Materials

Arundo donax shives used in this study were collected in west Hungary (Sopron) and subsequently conditioned and stored under controlled dry laboratory conditions prior to use. Prior to composite production, the Arundo donax shives were characterized to ensure material uniformity and reproducibility. Considering the elongated and anisotropic morphology of the shives, a combined methodology incorporating sieve analysis and digital image analysis was adopted. Sieve analysis was conducted on a representative 50 g sample obtained via random sampling. The test was performed using a mechanical sieve shaker at medium intensity (level 6) for 8 min, employing a standard stack of sieves with decreasing mesh sizes. The mass retained on each sieve was recorded, and the percentage retained, cumulative retained, and percentage passing were calculated. The results are summarized in Table 1, and the corresponding cumulative particle size distribution is presented in Figure1(a). However, due to the elongated, rod-like geometry of the shives, the sieve analysis does not reflect the actual particle length. Instead, it represents the minimum transverse dimension (width) controlling particle passage through the sieve openings. To provide a more comprehensive morphological characterization, digital image analysis was performed using ImageJ software (National Institutes of Health, USA) [27]. Images were acquired with a calibrated metric reference to ensure accurate spatial scaling. Given the irregular geometry and potential overlap of particles, a manual measurement approach was adopted [28]. A total of 869 particles were analysed, and for each particle, the maximum longitudinal length (L) was measured ((Fig. 1b). The results showed a mean length of 5.03 mm. This combined approach allows the sieve analysis to describe grading in terms of

Table 1
Sieve analysis of Arundo shives.

Sieve size (mm)	Mass retained (g)	% retained	Cumulative % retained	% passing	Relative error %
5	1.241	2.50	2.50	97.50	8.06
3	30.000	60.36	62.85	37.15	0.33
2	1.700	3.42	66.27	33.73	5.88
1	9.696	19.51	85.78	14.22	1.03
0.5	5.373	10.81	96.59	3.41	1.86
0.25	0.926	1.86	98.45	1.55	10.8
Bottom pan	0.768	1.55	100.00	-	13.0

Note: Relative error (%) = (balance accuracy / mass retained) × 100. Weighted by mass fraction, the overall mass distribution measurement accuracy is ±1.4%

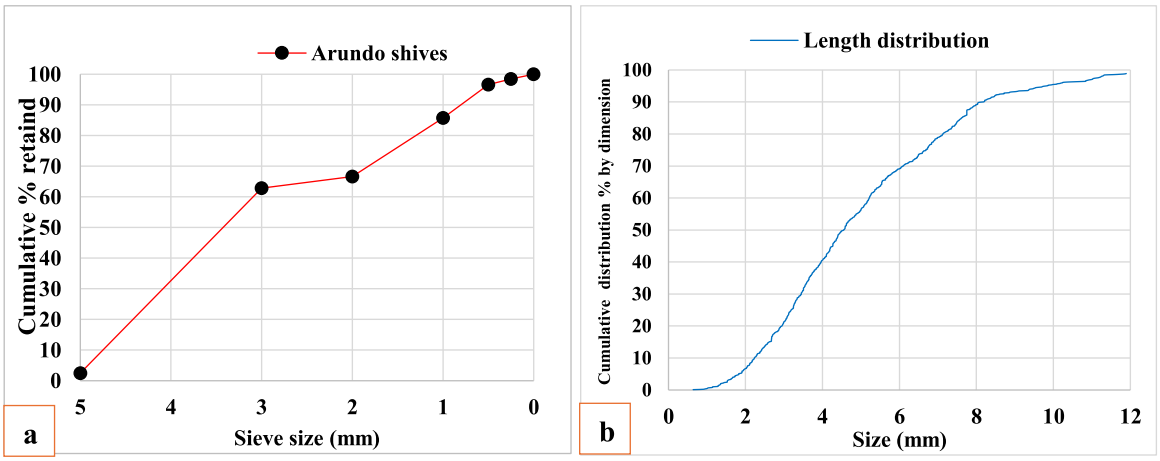

Fig. 1. cumulative % retained curve from sieve analysis [a], Cumulative size distribution curves for elongated particles [b] (Y-axis: The distribution is based on particle count (n = 869), showing the percentage of particles with dimensions smaller than the corresponding size on the X-axis).

transverse dimensions relevant to packing behavior, while image analysis provides information on particle length.

The binder used in this study was a commercially available high-calcium hydrated lime purchased in Sopron, Hungary. The material conforms to the EN 459–1:2015 standard, classified as a non-hydraulic aerial lime. Table (2) shows physical and chemical properties of the commercial hydrated lime (CL 90-S) used in this study compared to the minimum requirements of the EN 459–1:2015 standard [29]. Lime was selected due to its proven compatibility with plant-based aggregates, vapor permeability, and suitability for bio-based composite applications. Tap water was used as the mixing medium for all formulations. An overview of the complete experimental workflow including raw material collection, material preparation, mixing and casting, curing and preconditioning, and subsequent experimental testing is provided in Fig. 2.

2.2. Mix Design and Sample Preparation

Three different binder-to-shive mass ratios were investigated in this study in order to evaluate the influence of binder content on the physical and thermal properties of Arundo donax shive–lime composites. The compositions were designated as Mix A, Mix B, and Mix C, as summarized in Table 3. For all mixtures, a constant water-to-binder ratio of 1.2:1 was maintained to ensure comparable workability and to isolate the effect of binder proportion.

The required quantities of Arundo donax shives and slaked lime were first dry-mixed to achieve a homogeneous distribution of the binder within the plant aggregate. Subsequently, the predetermined amount of water was gradually added while gently mixing the fresh composite by hand in order to avoid damage to the fibrous structure of the shives. After water addition, the mixtures were allowed to rest for several minutes to promote initial wetting and binder–aggregate interaction.

The fresh composites were then cast into rigid molds with dimensions of 300 mm × 300 mm × 30 mm (Fig. 2). The selected specimen dimensions were specifically designed to meet the requirements of the Hot Plate Method thermal conductivity apparatus and to ensure one-dimensional heat flow during testing. To mitigate heterogeneity concerns, maximum aggregate size was almost limited to approximately 10 mm, maintaining a 3:1 thickness-to-aggregate ratio. During casting process light manual compaction was applied to ensure uniform mold filling while preserving the intrinsic porosity characteristic of bio-based insulation materials. The specimens were demolded after 48 h and subsequently cured under laboratory conditions at an ambient temperature of 23 ± 2 °C and a relative humidity of 60% ± 5 for a period of 28 days prior to testing. These conditions were maintained using standard laboratory environmental control, with the observed fluctuation of the room environment.

Table 2
Key technical properties of the hydrated lime (CL 90-S) binder.

Property (Unit)	EN 459–1 Requirement [654]	Manufacturer Data (HU)
Total CaO + MgO	≥ 90.0%	94.5% – 97.2%
Carbon Dioxide (%)	≤ 4.0%	1.2% – 1.8%
Fineness (on 0.09 mm)	≤ 7.0%	3.5% – 5.0%
Bulk Density (Loose)	(Informative)	400 – 600 kg m^{-3}

2.3. Testing procedures

2.3.1. Physical property tests

2.3.1.1. Apparent (Bulk) density. The apparent (bulk) density of the Arundo donax shive–lime composite specimens was determined after 14 and 28 days of curing for each binder-to-shive ratio, in accordance with EN 1602.Prior to testing, all specimens were stored in a conditioned laboratory environment to minimize the influence of moisture variations on mass measurements. Specimen dimensions were measured using a digital calliper (± 0.02 mm), and mass was determined using a precision electronic balance (± 0.1 g).

The bulk density was calculated as the ratio of specimen mass to its total volume, including the solid matrix as well as internal pores and voids, using Eq. (1):

$$\rho = \frac{m}{V} \tag{1}$$

Where m is the mass of the specimen (kg) and V is the total specimen volume (m^3)

A total of three specimens were tested for each sample type (binder ratio) and average values are reported to ensure statistical reliability. The combined uncertainty was calculated using the root-sum-square (RSS) method, incorporating both instrument precision and experimental variability, using Eq. (2).

$$u_c = \sqrt{{u_{SD}}^2 + {u_{inst}}^2} \tag{2}$$

Where u_c is combined uncertainty, u_{SD} is random uncertainty and u_{inst} is instrument uncertainty

2.3.1.2. Water absorption. Following the curing period, specimens were oven-dried at 40 ± 2 °C until a constant mass (change <1% over 24 h) was achieved, establishing the initial dry mass (m_1). Water absorption was evaluated via immersion following the principles of ASTM C1763.

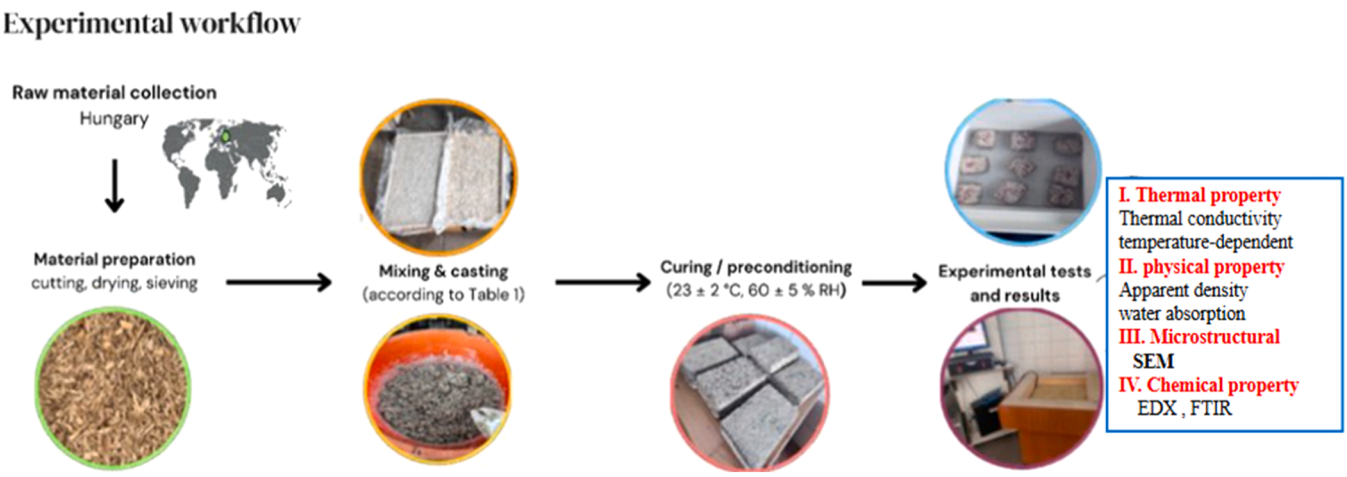

Fig. 2. Overview of the experimental workflow.

Table 3
Mix proportions of Arundo donax shive–lime composites.

Mix ID	Shive	Binder	Water	Binder/Shive	Water/Binder
A	1.0	1.0	1.2	1.0	1.2
B	1.0	1.5	1.8	1.5	1.2
C	1.0	2.0	2.4	2.0	1.2

This method involves complete immersion of the specimens in water and periodic determination of mass gain over time. The tests were conducted on rectangular prism specimens (100 ×100 x 50 mm), with three replicates tested for each binder ratio. All specimens were oriented such that the primary immersion axis was parallel to the pouring direction used during casting. Measurement uncertainty was minimized using a high-precision balance (balance with a resolution of 0.01 g) and surface-drying protocols.

Previous studies on hemp–lime composites have reported rapid water uptake during the initial stages of immersion [48]. To capture this early-stage absorption behaviour more accurately, additional measurement intervals were introduced prior to the conventional 24 h reading. Mass measurements were therefore recorded after 1 h, 2 h, 3 h, 4 h, 12 h, 24 h, and 48 h of immersion.

The water absorption percentage (W_A, %) was calculated using Eq. (3):

$$W_A(\%) = \frac{m_2 - m_1}{m_1} x \quad 100 \tag{3}$$

where m_1 is the oven-dried mass of the specimen (kg) and m_2 is the mass after immersion at the specified time interval (kg).

2.3.2. Thermal property test

The thermal conductivity (λ) of the composite specimens was determined using a laboratory-built and calibrated guarded hot plate apparatus (accuracy ±2%) in accordance with EN 12667 (and ISO 8301). In this method, a steady-state heat flow is established through the specimen by supplying a known electrical power to the main heater, and the resulting heat flux is calculated from this electrical input and the metering area of the apparatus.

Initially, a constant temperature gradient was established across the specimen thickness (d) by maintaining the hot and cold plates at 15 °C and 5 °C, respectively, resulting in a mean temperature (T_mean) of approximately 10 °C. After reaching steady-state conditions (defined as a fluctuation of less than 0.002 $W{\cdot}m^{-1}{\cdot}K^{-1}$ within 10 min), measurements were initiated, and temperature and electrical power data were recorded at one-minute intervals. The reported thermal conductivity values represent the average of 100 consecutive measurements (i.e., 100 min of data acquisition).

To minimize potential thermal hysteresis effects and ensure measurement reproducibility, a sequential temperature protocol was applied. The apparatus was equipped with 15 cm thick lateral insulation to promote one-dimensional heat transfer through the specimen. To ensure statistical reliability, three independent samples were tested for each binder-to-shive ratio.

To account for material anisotropy, specimens were oriented with their top faces parallel to the original casting direction, corresponding to their intended application as wall insulation. Temperature-dependent thermal conductivity was measured over a range from −10 °C to 50 °C in 10 °C increments on the cold side, while maintaining a constant temperature difference of 10 °C between the hot and cold plates. At each setpoint, steady-state conditions were ensured before recording measurements.

The steady-state thermal conductivity (λ) was calculated from the heat flux, derived from the electrical power input, the specimen thickness, and the temperature difference (ΔT) across the sample, as expressed in Eq. (4):

$$\lambda = \frac{qxd}{\Delta T} \tag{4}$$

where λ is the thermal conductivity ($W{\cdot}m^{-1}{\cdot}K^{-1}$), q is the heat flux density ($W{\cdot}m^{-2}$) calculated from the supplied electrical power, d is the specimen thickness (m), and ΔT is the temperature difference between the plates (K).

Because of the moisture content of the materials affect thermal conductivity the samples were measured before the measurement and after measurement to be sure the moisture content does not change significantly. Mass variations before and after temperature-dependent measurements were below 0.5%, indicating negligible moisture exchange.

2.3.3. Microstructural and Chemical Characterization (SEM, EDX, and FTIR)

The microstructural and chemical characteristics of Arundo donax shives before and after incorporation into the lime matrix were investigated using scanning electron microscopy (SEM), energy-dispersive X-ray spectroscopy (EDX), and Fourier Transform Infrared (FTIR) spectroscopy. SEM observations were performed using a HITACHI S-3400N scanning electron microscope operated under low-vacuum conditions, without conductive coating, enabling direct examination of the native surface morphology. Elemental and qualitative chemical analyses were carried out using an EDX system (Bruker) coupled to the SEM. FTIR measurements were conducted using a JASCO FT/IR-6300 spectrometer

in attenuated total reflectance (ATR) mode to examine chemical structure before and after lime incorporation. Spectra were collected over the range 4000–400 cm^{-1} with a resolution of 4 cm^{-1} , averaging 50 scans per sample, and background correction was applied prior analysis.

3. Results and discussion

3.1. Apparent (Bulk) density

Table (4) and Fig. (3) present the apparent (bulk) density of the Arundo donax shive–lime composites as a function of binder-to-shive ratio and curing time. As expected, the apparent density increased with increasing binder content and decreased with curing time for all mixtures.

In bio-based composites, density variations are fundamentally driven by microstructural porosity, where lower density indicates a more open pore network, and higher density reflects reduced pore volume due to binder infiltration and matrix densification. This relationship is consistent with findings in bio-based composites, where porosity is the dominant factor controlling both density and functional performance [15,16].

After 14 days of curing, the average apparent densities were 326 ± 4.61 kg m^{-3} , 407 ± 1.00 kg m^{-3} , and 488 ± 6.65 kg/m^3 for binder-to-shive ratios of 1:1, 1.5:1, and 2:1, respectively. Between 14 and 28 days, a consistent reduction in density was observed across all formulations. Specifically, the density of the 1:1 mixture decreased from 326 ± 4.61–302 ± 4.95 kg m^{-3} , corresponding to a reduction of 7.36%. Similarly, the 1.5:1 mixture exhibited a decrease from 407 ± 1.00–376 ± 2.45 kg m^{-3} (7.62%), while the 2:1 mixture showed the largest reduction, decreasing from 488 ± 6.65–445 ± 3.20 kg m^{-3} (8.81%).

As free and chemically unbound water is gradually released from the lime matrix, the sample undergoes mass loss due to evaporation. Simultaneously, drying shrinkage reduces the physical dimensions of the samples [30]. The observed decrease in apparent density is primarily attributed to moisture loss during drying, which reduces specimen mass. The higher percentage reduction observed in mixtures with greater binder content suggests that these formulations initially retain larger amounts of water, resulting in more pronounced mass loss during the curing process.

At 28 days, the apparent densities ranged from 302 ± 4.95–445 ± 3.20 kg/m^3 , which is approximately 16–50% lower than those reported for conventional lignocellulosic particleboards and 10–14% lower than values commonly reported for other bio-based insulation materials, such as hemp–lime composites [20,31,33]. This relatively low density is advantageous for thermal insulation applications, as it limits conductive heat transfer and increases the volume of entrapped air within the composite matrix.

Among the investigated formulations, the binder-to-shive ratio of 1.5:1 appears to provide an optimal balance between density, porosity, and material cohesion. This mixture achieves sufficient binding and structural integrity while maintaining a moderate density reduction conducive to enhanced thermal insulation performance. Consequently, the 1.5:1 composition may represent a favourable compromise between mechanical stability and thermal efficiency for practical building insulation applications.

Table 4
Apparent Density Results of Arundo donax–Lime Composites.

Binder/ Shive	Sample	Weight (kg) 14 d	Weight (kg) 28 d	Apparent Density (kg·m^{-3}) 14 d	Apparent Density (kg·m^{-3}) 28 d
1:1	Average	0.880	0.817	326.06	302.15
	SD	0.012	0.013	4.61	4.95
1.5:1	Average	1.099	1.014	407.16	375.79
	SD	0.003	0.007	1.00	2.45
2:1	Average	1.317	1.203	487.81	445.36
	SD	0.019	0.008	6.65	3.20

3.2. Water absorption behaviour

Fig. 4 illustrates the water absorption behaviour of the Arundo donax shive–lime composites as a function of immersion time for different binder-to-shive ratios. All mixtures exhibited rapid initial water uptake, with the majority of absorption occurring within the first 1–4 h of immersion. This initial phase was followed by a progressively slower increase in mass, approaching equilibrium conditions after approximately 24–48 h.

A clear inverse relationship between water absorption capacity and binder-to-shive ratio was observed. Specimens with the lowest binder content (1:1) showed the highest water uptake, reaching approximately 120.33% after 24 h of immersion. This pronounced absorption can be attributed to the high open porosity of the composite and the incomplete encapsulation of Arundo donax shives by the lime matrix, which facilitates rapid capillary water ingress. In contrast, composites with higher binder content (2:1) exhibited substantially reduced water absorption, limited to approximately 50.83%, reflecting improved matrix continuity, reduced interconnected pore volume, and partial blockage of capillary pathways.

The observed absorption trends are consistent with previously reported behavior for other plant-based lime composites, such as hemp–lime, which are known for their strong hygroscopic nature and rapid early-stage water uptake. While this moisture sensitivity can pose challenges for applications directly exposed to water, it may also contribute to favorable hygrothermal regulation when used in protected building envelope systems.

Overall, the results indicate that although Arundo donax–lime composites demonstrate strong potential as sustainable thermal insulation materials, their moisture-related behavior must be carefully considered in design and application. Appropriate detailing, surface protection, or the use of higher binder contents may be required to mitigate excessive water absorption in moisture-prone environments.

3.3. Thermal conductivity

Fig. 5 shows the thermal conductivity (λ) of Arundo–lime composites after 28 days of curing. Thermal conductivity increases with increasing binder-to-shive ratio, with mean values of 0.072 ± 0018, 0.083 ± 0.0017, and 0.092 ± 0.0012 $W{\cdot}m^{-1}{\cdot}K^{-1}$ for the 1:1, 1.5:1, and 2:1 mixtures, respectively. The 2:1 formulation exhibits a 27.7% higher λ than the 1:1 mixture. This increase is attributed to microstructural densification at higher binder contents, where enhanced carbonation and partial pore filling reduce air-filled porosity and promote solid-phase heat transfer. Heat transfer in porous bio-based composites occurs through a combination of solid-phase conduction, gas conduction within pores, and radiative transfer. As binder content increases, the continuity of the solid phase improves, enhancing conductive heat transfer, while the reduction in pore connectivity limits the insulating effect of entrapped air. Consequently, mixtures with lower binder content retain a more open pore network and exhibit superior insulation performance. This inverse relationship between porosity and thermal conductivity is widely reported in bio-based materials [21,22], confirming that the reduction of air-filled voids leads to increased thermal conductivity.

The porosity of Arundo–lime composites was quantified using color-segmented digital image analysis (ImageJ) on red-dyed samples. By applying HSB thresholding to isolate pore regions, where porosity was calculated as the ratio of pore area to total sample area. The analysis revealed porosity ranges between 53% and 80%. These results align with the composites measured density (302–445 kg·m^{-3}), suggesting a total porosity of approximately 60–80%, consistent with similar lignocellulosic systems [34,35]. The incorporation of lime binder progressively reduces this porosity through coating of particle surfaces and partial

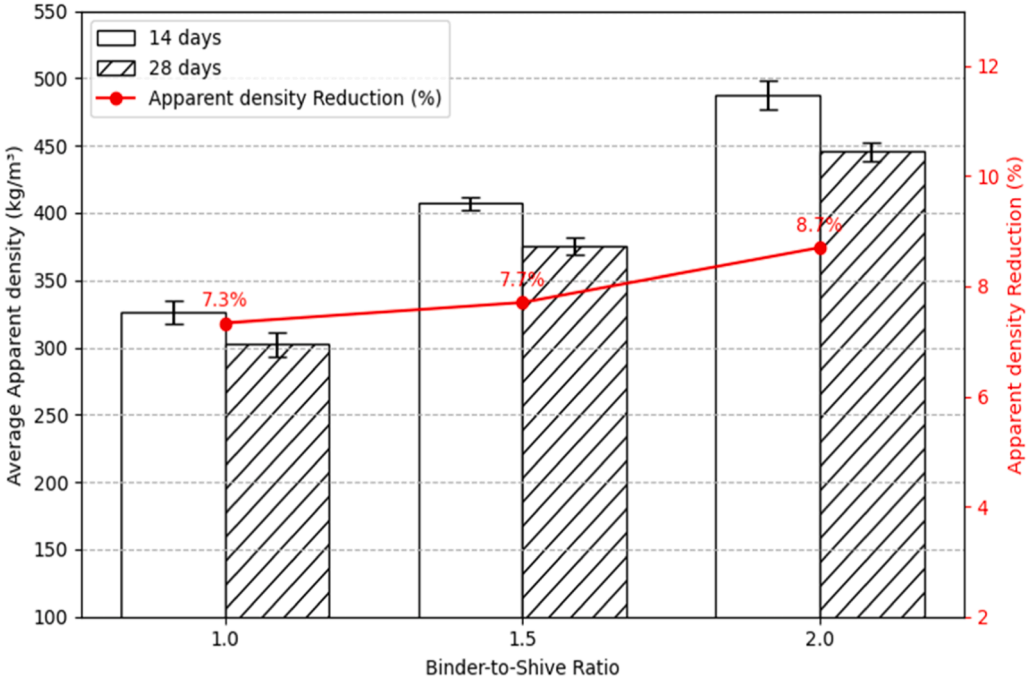

Fig. 3. Average apparent density of specimens at 14 and 28 days across different binder-to-shive ratios. Error bars represent the combined uncertainty (u_c) based on standard deviation and instrument resolution.

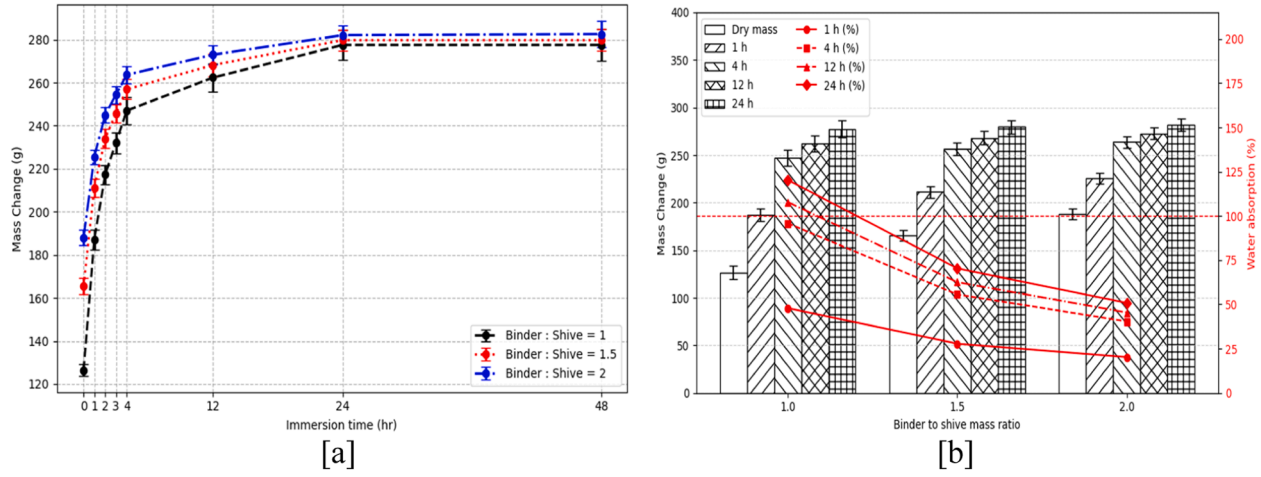

Fig. 4. Water absorption behavior of Arundo donax–lime composites: [a] mass change as a function of absorption time (h); [b] mass change and percentage of water absorption. Error bars represent ± standard deviation (SD)(n = 3).

filling of internal voids, as confirmed by SEM observations. This reduction in pore volume increases the continuity of the solid phase and enhances heat transfer through the matrix. Piątkiewicz et al. reported that thermal conductivity grows with increasing binder-to-shiv ratio up to ~20% increase with more binder content [35]. Therefore, the observed increase in thermal conductivity with binder content can be directly linked to a decrease in effective porosity and an increase in solid-phase conduction pathways. Similar trends have been reported for hemp–lime and reed-based composites, where thermal conductivity increases with decreasing porosity and increasing density [36–38].

A strong linear relationship between apparent density and thermal conductivity was observed, described by

$$\lambda = 1.45 \times 10^{-4}\,\rho - 0.0286 \quad (R^2 \approx 0.99)$$

where ρ is the dry density (kg·m^{-3}). The regression indicates an increase of approximately 0.0145 W·m^{-1} ·K^{-1} in λ for every 100 kg·m^{-3} increase in density, confirming density as the dominant factor governing heat transfer. This strong linear relationship confirms that density can be used as a reliable predictor of thermal conductivity in such composites. Since density is inversely related to porosity, this relationship further supports the conclusion that thermal conductivity is primarily controlled by the internal pore structure. This behaviour is consistent with classical models for porous materials, where heat transfer depends on the volume fraction and connectivity of the solid and gaseous phases, as well as with reported results for bio-based composites [15,16].

Thermal conductivity is not constant with temperature, however the EN 12667 standard determines only one temperature range, but the value can be significantly different in other temperature range. Usually thermal conductivity increases with temperature, but the slope and linearity of the curve are already material characteristics. To determine the effect of moisture exchange during testing, mass was recorded before and after the full temperature cycle, and it was with variations below

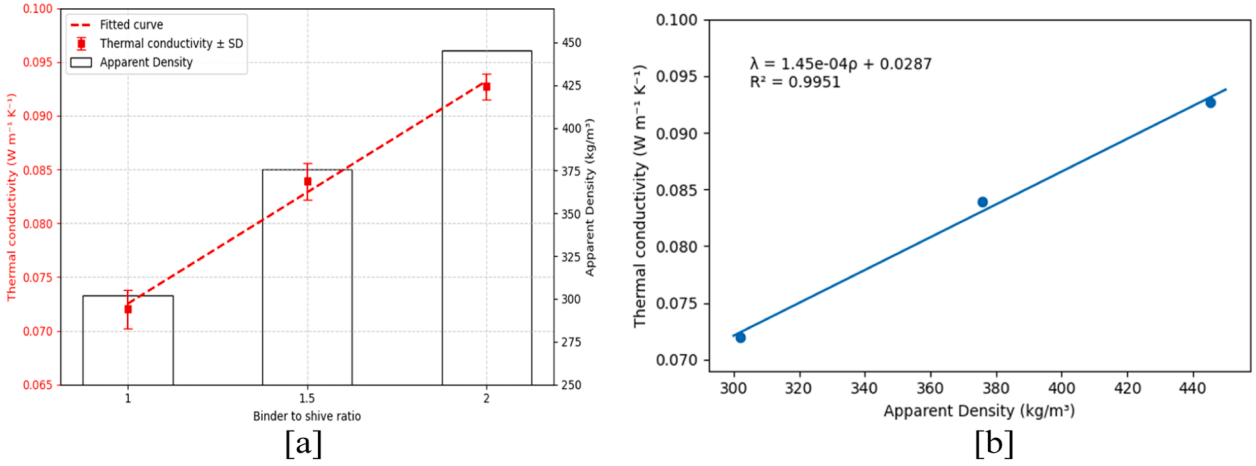

Fig. 5. Thermal conductivity of Arundo donax–lime composites: (a) Thermal conductivity as function of binder to shive ratio; (b) linear relationship between apparent density and thermal conductivity. Error bars represent ± standard deviation (SD) (n = 3).

0.5%, indicating negligible moisture loss or gain during testing. This confirming that any observed changes in thermal conductivity are primarily temperature driven.

Temperature-dependent thermal conductivity data (Fig. 6) show a progressive increase in λ over the investigated temperature range for all mixtures. This behaviour is consistent with literature on porous insulating materials and can be attributed to several mechanisms. The increase in thermal conductivity with temperature is attributed to enhanced molecular activity in both solid and gaseous phases, as well as increased radiative heat transfer within the pore network [39].

At any given temperature, higher binder contents yield higher λ values due to increased density and reduced air-filled porosity. The 1:1 mixture exhibits the lowest thermal conductivity across the entire temperature range, reflecting its more open pore structure. Linear regression analysis indicates that temperature sensitivity decreases with increasing binder content. The 1:1 ratio shows the highest sensitivity, followed by the 1.5:1 ratio, while the 2:1 ratio exhibits the lowest sensitivity and the most linear behaviour:

$$\lambda = 1.06 \times 10^{-2}\, T - 0.0433 \quad (R^2 \approx 0.84) \quad (1:1\text{ratio})$$

$$\lambda = 6.6 \times 10^{-3}\, T - 0.0607\text{with}(R^2 \approx 0.93) \quad (1.5:1\text{ratio})$$

$$\lambda = 4.6 \times 10^{-3}\, T - 0.0811\text{with}(R^2 \approx 0.99) \quad (2:1\text{ratio})$$

The decrease in temperature sensitivity with increasing binder content can be explained by the reduction in porosity and increased structural uniformity. In highly porous materials, heat transfer is more sensitive to temperature due to the dominant role of air within the pore network. As porosity decreases, the contribution of the solid phase becomes more significant, resulting in more stable and less temperature-dependent thermal behaviour.

Overall, thermal conductivity increases linearly with temperature for all formulations, while the temperature sensitivity ($(\frac{d\lambda}{dT})$) decreases systematically with increasing binder content (1:1 > 1.5:1 > 2:1). The largest differences between mixtures are observed at lower temperatures, where the influence of pore structure is more pronounced, while at higher temperatures, the values converge due to the increasing contri-

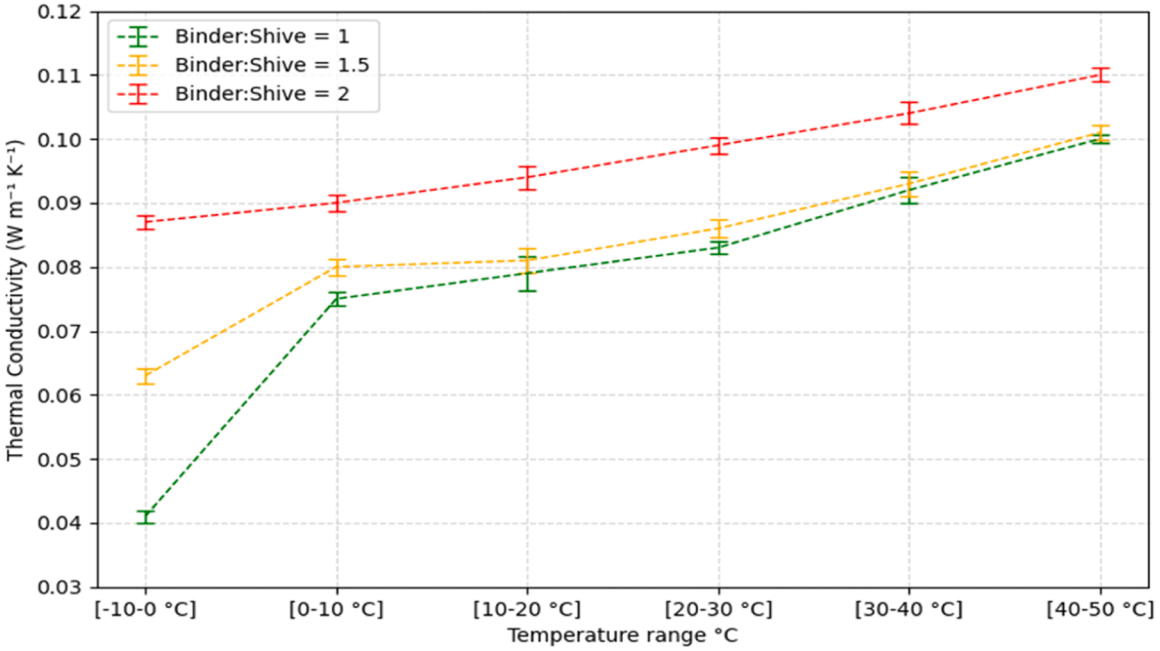

Fig. 6. Temperature-dependent thermal conductivity (Error bars represent ± (SD) (n = 3)).

bution of temperature-dependent heat transfer mechanisms.

3.4. Microstructural and Chemical Analysis (SEM, EDX, FTIR)

3.4.1. SEM analysis

The surface morphology of raw Arundo donax shives (Fig. 7a) reveals a highly porous and fibrous microstructure. As indicated by arrows (A1–A3), the raw particles exhibit (A1) well-defined longitudinal grooves and fiber alignment, (A2) large open lumens and interconnected voids, and (A3) rough, irregular surfaces with micro-cracks. These features are characteristic of lignocellulosic biomass and contribute to high water absorption and low density, while providing pathways for binder penetration [40].

In Fig. 7b, the SEM micrographs of the 1.5:1 binder-to-shive ratio Shive reveal significant microstructural transformations. Arrows (B1–B3) highlight (B1) the formation of a continuous mineral coating, (B2) the partial filling and blockage of lumens and pores, and (B3) a denser, more compact matrix surrounding the shives. These observations suggest improved particle–matrix bonding and a marked reduction in accessible porosity.

This behavior aligns with studies on bio-aggregates, where mineral binders penetrate the cellular structure of the fibers, leading to densification and reduced permeability [21,41].These microstructural modifications explain the recorded reduction in water absorption and the increase in thermal conductivity; as the binder fills the air-filled voids, it enhances the solid-phase heat transfer across the composite [41].

3.4.2. EDX analysis

Elemental analysis of raw shives (Fig. 8a; Table 5) confirms a lignocellulosic composition dominated by carbon (49.2 wt%) and oxygen (44.6 wt%), with minor nitrogen (4.4 wt%) and trace inorganic elements (Si, Na, Mg, P). No calcium was detected, confirming the absence of mineral binder prior to incorporation.

In the lime-containing shive of (1.5:1) binder-to-shive ratio sample (Fig. 8b; Table 5), calcium is clearly observed (6.8 wt%), while the relative carbon content decreases and oxygen increases, reflecting the addition of oxygen-rich mineral phases. Minor magnesium and silicon signals persist, and the appearance of calcium provides direct evidence of effective binder coating and integration. These compositional changes support the SEM observations of pore filling and densification, explaining the associated increases in density and thermal conductivity and the reduction in water absorption.

3.4.3. FTIR analysis

The FTIR spectra in Fig. 9 demonstrate significant physicochemical interactions between raw Arundo shives and the lime incorporated shive of 1.5:1 binder to shive ratio. A pronounced reduction and shift in the broad O–H stretching band (3200–3600 cm^{-1}) is observed in lime incorporated shive, indicating substantial modification of hydroxyl environments under highly alkaline conditions. This behavior suggests deprotonation and partial consumption of hydroxyl groups, accompanied by a disruption of intermolecular hydrogen bonding. Such spectral changes are consistent with previous studies, where alkaline media ($Ca(OH)_2$) alter OH vibrational characteristics and weaken hydrogen-bonding networks [42,43].

Alterations in the carbonyl region (~1700 cm^{-1}), particularly the attenuation of bands associated with acetyl and ester groups, indicate alkaline hydrolysis of hemicellulose. This aligns with reported behavior of lignocellulosic fibers in calcium-rich alkaline environments, where hemicellulose degradation occurs alongside the formation of calcium–carboxylate interactions [44]. These chemical transformations enhance fiber surface reactivity and promote improved interfacial adhesion within the composite matrix. Additionally, increased absorption in the 1400–1500 cm^{-1} region is attributed to asymmetric stretching vibrations of carbonate ions (CO_3^{2-}), confirming the formation of calcium carbonate ($CaCO_3$) through lime carbonation. This observation is supported by established carbonation mechanisms in lime-based systems [45]. Small fluctuations in the fingerprint region (500–800 cm^{-1}) further support the presence of crystalline carbonates without the introduction of extraneous functional groups.

Overall, these spectral modifications confirm strong chemical interactions between lime and Arundo shives, including hydroxyl modification, hemicellulose degradation, and carbonate formation. Together, these processes contribute to enhanced interfacial bonding, matrix densification, and improved structural continuity, ultimately supporting the mechanical integrity and thermal performance of the developed biocomposite.

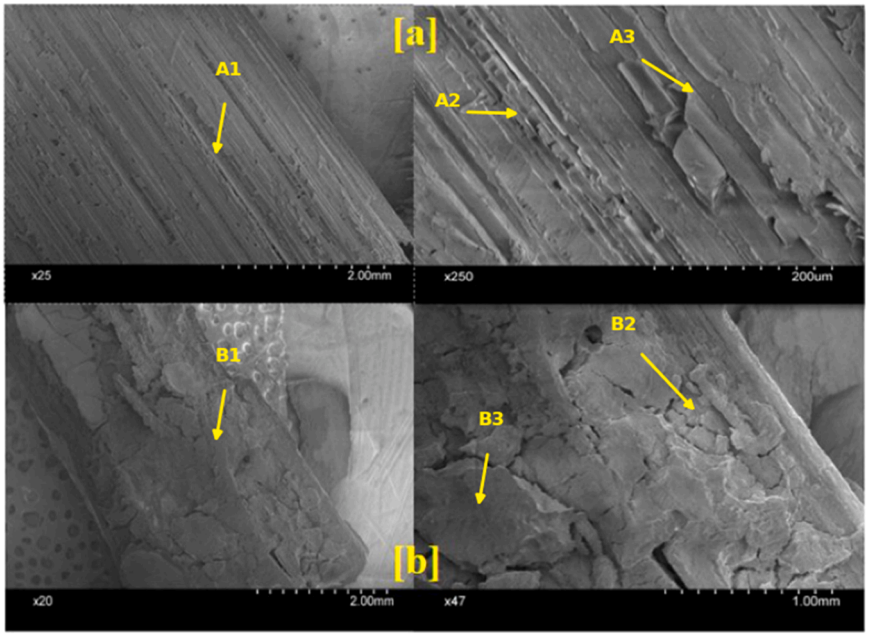

Fig. 7. SEM micrographs of the (1.5:1) binder-to-shive ratio Shive [a] before and [b] after lime incorporation, shown at various magnifications.

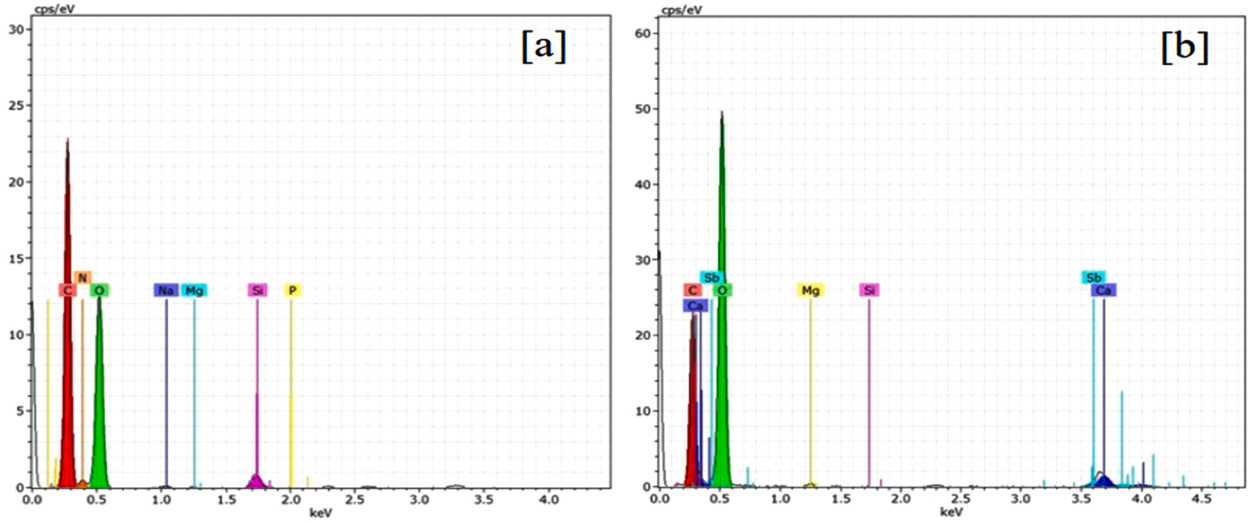

Fig. 8. EDX spectra of Arundo donax shives with a 1.5:1 binder-to-shive ratio [a] before and [b] after lime incorporation.

Table 5
EDX elemental composition of raw and lime incorporated Arundo donax shives.

Raw Arundo donax shive sample			Lime incorporated Arundo donax shives sample (binder/shive 1.5:1)	
Element	[norm. wt%]	[norm. at%]	[norm. wt%]	[norm. at%]
Carbon	49.21	56.42	25.37	34.24
Oxygen	44.58	38.37	61.27	62.07
Calcium	0	0	6.79	2.75
Magnesium	0.03	0.02	0.13	0.08
Silicon	1.66	0.81	0.02	0.01
Nitrogen	4.38	4.31	0	0
Antimony	0	0	6.42	0.85
Sodium	0.10	0.06	0	0
Phosphorus	0.03	0.01	0	0
Sum:	100	100	100	100

4. Comparison with existing literature

The measured densities and thermal conductivities of the Arundo donax shive–lime composites developed in this study are in good agreement with values reported in the literature for reed- and hemp-based bio-aggregate materials (Fig. 10). The apparent densities measured at 14 days align well with previously published results for Arundo-based composites. For example, Cintura et al. [31] reported apparent densities of approximately 517 kg·m^{-3} for Arundo-based panels, which are comparable to the mid-range densities observed in the present study at higher binder contents. In contrast, significantly higher densities (735–913 kg·m^{-3}) have been reported for binderless Arundo particleboards manufactured by hot-pressing [47], reflecting fundamentally different processing routes and compaction levels, although the purpose of this panels were not thermal insulation.

The 28-day densities obtained in this work (302–445 kg·m^{-3}) are

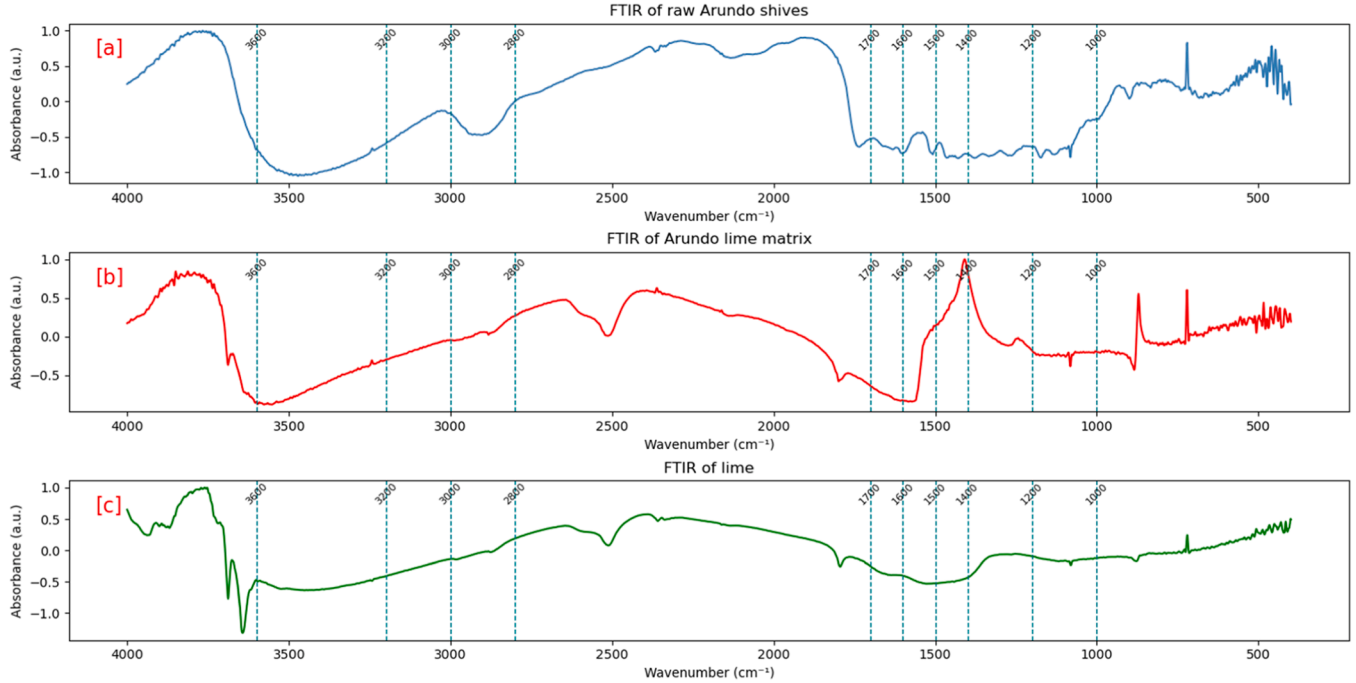

Fig. 9. FTIR spectrum of Arundo shives[a], Arundo lime matrix [b] and Lime [c].

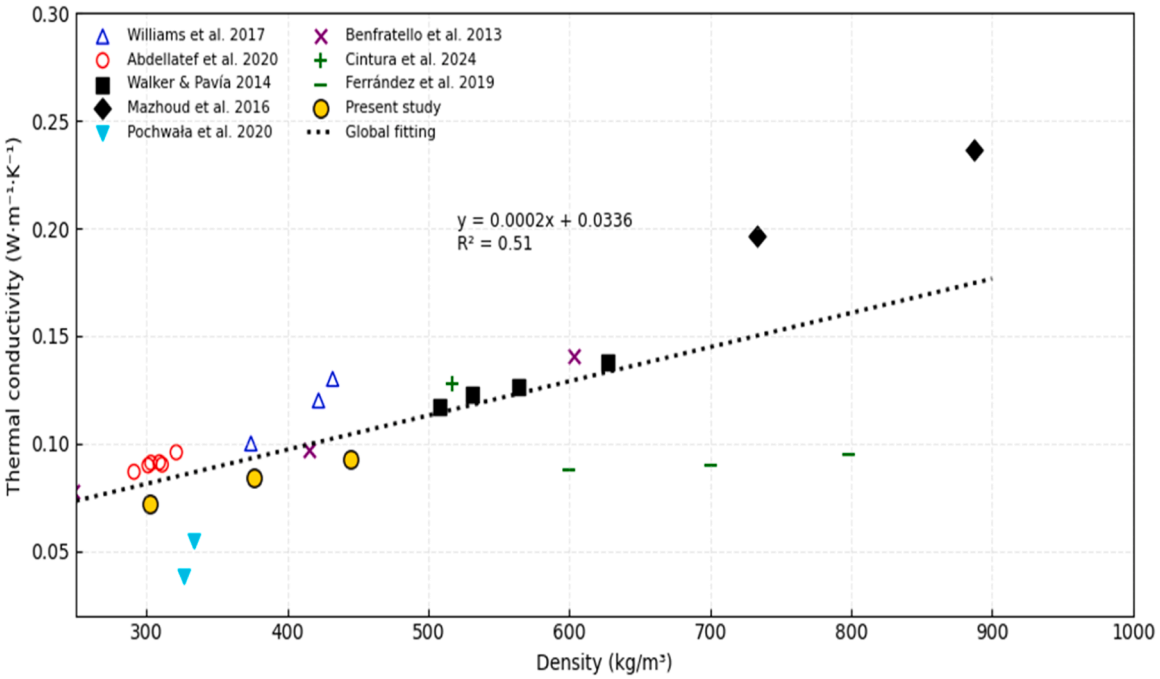

Fig. 10. Thermal conductivity and density comparison with other study.

substantially lower than those reported for most particleboard-type Arundo materials, confirming the lightweight nature of the composites produced here and their suitability for thermal insulation applications. Lower density is advantageous from a thermal perspective, as increased porosity and reduced solid fraction generally limit conductive heat transfer. Importantly, even at higher binder-to-shive ratios, the composites retained relatively low densities, indicating that sufficient matrix continuity and cohesion can be achieved without excessive mass. This characteristic is particularly relevant for sustainable building envelope systems, where low self-weight and reduced material consumption are desirable.

The thermal conductivity values measured in this study (λ = 0.072–0.092 $W{\cdot}m^{-1}{\cdot}K^{-1}$ for densities of approximately 302–445 $kg{\cdot}m^{-3}$) fall well within the range reported for Arundo- and hemp-based bio-aggregate composites. The thermal performance of Arundo donax–based composites is strongly governed by moisture content due to their hygroscopic and highly porous structure. Cintura et al. (2023) found that Arundo donax -based composites combine low thermal conductivity with pronounced hygroscopic behavior, implying a potential influence of environmental humidity on heat transfer, although this relationship was not explicitly quantified [49]. This moisture sensitivity is further supported by Nicoletti et al. (2015), who demonstrated that increasing moisture content alters the mechanical and viscoelastic properties of Arundo donax, suggesting underlying structural changes that may also affect heat transfer mechanisms [50]. In lime-based composites, Pavlík et al. (2009) quantified a marked increase in thermal conductivity with increasing moisture content, attributed to the replacement of air by water within the pore network, thereby enhancing conductive heat pathways [51]. Similarly, Malheiro et al. (2021) showed that reed-based materials exhibit moisture-dependent physical and thermal properties, with higher water content leading to increased thermal conductivity [52]. These findings are consistent with broader analyses of bio-based insulation systems, where hygroscopic materials demonstrate a systematic rise in thermal conductivity with moisture uptake due to coupled heat and moisture transfer processes [53]. Collectively, these studies indicate that while Arundo donax–lime composites provide effective insulation in dry conditions, their in-service thermal conductivity is expected to increase with moisture content, highlighting the importance of hygrothermal considerations in their practical application. The relationship between moisture content and thermal conductivity remains insufficiently explored within the scope of this study, highlighting the need for further investigation.

Despite this limitation, the thermal conductivity values obtained in this study are consistent with those reported in the literature for similar reed-based materials. Ferrández-García et al. (2019) reported λ values between 0.081 and 0.093 $W{\cdot}m^{-1}{\cdot}K^{-1}$ for giant reed boards with comparable densities, concluding that reed-based materials exhibit suitable insulation performance [32]. Similarly, Cintura et al. (2024) and other recent studies have reported λ values approaching 0.12 $W{\cdot}m^{-1}{\cdot}K^{-1}$ for Arundo-based composites with densities close to 500 $kg{\cdot}m^{-3}$, which is consistent with the density-dependent increase in thermal conductivity observed in the present work [31].

When compared with the broader literature on hemp–lime and other plant-aggregate lime composites, the thermal performance of the Arundo–lime system investigated here can be considered broadly comparable. Very low thermal conductivity values occasionally reported for optimized hemp–lime formulations ($\lambda \approx$ 0.03–0.05 $W{\cdot}m^{-1}{\cdot}K^{-1}$) are typically associated with very low bulk densities (<350 $kg{\cdot}m^{-3}$), highly controlled mix designs and fibre from hemp, and specific processing techniques that may not reflect typical construction practice [18,19]. In contrast, a large body of experimental data for hemp–lime composites with densities in the range of approximately 300–500 $kg{\cdot}m^{-3}$ reports thermal conductivity values between 0.06 and 0.11 $W{\cdot}m^{-1}{\cdot}K^{-1}$ [20,33,46]. Within this context, the thermal conductivity values obtained for the Arundo–lime composites in the present study are fully consistent with those reported for mid-density plant-aggregate lime systems.

The observed increase in thermal conductivity with increasing binder content further aligns with established heat-transfer mechanisms in porous composites. The lime binder forms a continuous solid phase with a higher intrinsic thermal conductivity than air; consequently, increasing binder proportion enhances solid-phase connectivity while reducing the effective volume and connectivity of air-filled pores. Even when total porosity varies only moderately, changes in pore size distribution, pore connectivity, shive coating, and interfacial transition zones can lead to measurable increases in thermal conductivity. These microstructural considerations reinforce the interpretation of the

density–thermal conductivity relationship observed in this study and confirm its consistency with existing theoretical and experimental frameworks.

Compared with hemp–lime composites and other Arundo-based materials, the Arundo donax–lime composites investigated in this study exhibited water absorption behaviour that is consistent with values reported in the literature. Short-term immersion studies on hemp–lime composites typically report water uptake values in the range of approximately 30–60%, while longer immersion periods often result in cumulative absorption levels of 100–140% [18,20,31,33]. The relatively high-water uptake observed for the Arundo–lime composites during the initial 4 h of immersion can be attributed to the intrinsic hydrophilicity of Arundo shives, their elongated and fibrous morphology, and the presence of a highly interconnected open-pore network, which promotes rapid early-stage capillary absorption. Similar early-stage absorption behaviour has been widely reported for hemp–lime systems and other reed-based bio-aggregate composites.

Overall, the Arundo donax–lime composites developed in this study exhibit thermal conductivity, apparent density, and water absorption characteristics that are fully consistent but fall in the lower range with those reported for Arundo-, hemp-, and other reed-based lime composites. Among the investigated parameters, apparent density—governed primarily by binder content and resulting pore structure—emerges as the dominant factor controlling both thermal performance and moisture uptake behaviour. These findings confirm that Arundo–lime composites function effectively as mid-density bio-based insulation materials and demonstrate that Arundo donax represents a viable and regionally adaptable alternative to more established hemp–lime systems for sustainable building applications.

5. Conclusion

This study demonstrated that Arundo donax shive–lime composites are promising bio-based insulation materials. Increasing binder content raised apparent density and thermal conductivity while reducing water absorption, driven by matrix densification, partial pore filling, and progressive carbonation. After 28 days, densities ranged from 302 to 445 $kg{\cdot}m^{-3}$ and thermal conductivity from 0.072 to 0.092 $W{\cdot}m^{-1}{\cdot}K^{-1}$, with a strong linear correlation between density and conductivity ($R^2 \approx 0.99$). Temperature-dependent tests revealed increasing thermal conductivity with temperature, while higher binder contents reduced temperature sensitivity, indicating enhanced thermal stability.

SEM, EDX, and FTIR analyses confirmed effective lime coating, reduced porosity, and $CaCO_3$ formation, linking microstructural evolution to physical and thermal behavior. Water absorption decreased significantly with increasing binder ratio, consistent with improved matrix continuity.

While compared with existing hemp–lime and reed-based bio-aggregate composites, the Arundo donax -lime materials developed in this study exhibit comparable thermal and hygroscopic performance. Among the formulations, the 1.5:1 binder-to-shive ratio provided the best balance of low density, insulation performance, moisture resistance, and thermal stability.

Overall, Arundo donax is a viable, regionally adaptable alternative to conventional plant aggregates. To support real-world applications, future research should assess long-term durability and hygrothermal performance under cyclic conditions. Specifically, quantifying the internal pore size distribution and structure, which is essential to validate density-thermal relationships. Additionally, employing TGA and phenolphthalein staining will distinguish the impact of carbonation from mass loss due to moisture evaporation, allowing for more precise modelling of how the composite's microstructure evolves over time.

CRediT authorship contribution statement

Mebratu Tufa: Writing – original draft, Visualization, Methodology, Investigation, Formal analysis, Data curation, Conceptualization. **Zoltán Pásztory:** Writing – review & editing, Validation, Supervision, Resources, Methodology.

Declaration of Competing Interest

The authors confirm that this manuscript is original, has not been published previously, and is not under consideration for publication elsewhere. All authors have approved the submission and agree with its content. The authors understand that the journal may use plagiarism detection and screening tools to verify compliance with publishing policies. They also acknowledge and accept the journal's policies regarding publication and plagiarism.

Data availability

Data will be made available on request.

References

[1] Z. Ke, X. Liu, H. Zhang, X. Jia, W. Zeng, J. Yan, H. Hu, W.N. Hien, Energy consumption and carbon emissions of nearly zero-energy buildings in hot summer and cold winter zones of China (Article), Sustainability 15 (14) (2023) 11453, https://doi.org/10.3390/su151411453.
[2] A. Shahee, M. Abdoos, A. Aslani, R. Zahedi, Reducing the energy consumption of buildings by implementing insulation scenarios and using renewable energies (Article), Energy Inform. 7 (1) (2024) 18, https://doi.org/10.1186/s42162-024-00311-9.
[3] S.C. Füchsl, F. Rheude, H.J. Röder, Life cycle assessment (LCA) of thermal insulation materials: A critical review (Article), Clean. Mater. 5 (2022) 100119, https://doi.org/10.1016/j.clema.2022.100119.
[4] V. Cascione, M. Roberts, S. Allen, C. Charbel, D. Maskell, B. Dams, A. Shea, P. Walker, S. Emmitt, Evaluating environmental impacts of bio-based insulation materials through scenario-based and dynamic life cycle assessment, Int. J. Life Cycle Assess. 30 (2025) 601–620, https://doi.org/10.1007/s11367-024-02425-4.
[5] L. Cosentino, J. Fernandes, R. Mateus, A review of natural bio-based insulation materials, Energies 16 (12) (2023) 4676, https://doi.org/10.3390/en16124676.
[6] A. Yazdanseta, Y. Mi, Knowledge mapping for advancement of hemp-lime composite in the construction industry: A systematic literature review (from 2004 to 2024) (Article), J. Mater. Sci. Mater. Eng. 20 (2025) 115, https://doi.org/10.1186/s40712-025-00334-4.
[7] P. Cerny, M. Babenko, P. Bartos, Y. Kononets, P. Kriz, R. Rabenseifer, F. Spalek, Complex study of the composite building material based on flax straw organic waste: Hygrothermal and physicochemical properties, Waste Biomass-.-. Valoriz. 15 (4) (2024) 2231–2247, https://doi.org/10.1007/s12649-023-02273-7.
[8] K. Steyn, W. de Villiers, A.J. Babafemi, A comprehensive review of hempcrete as a sustainable building material (Article), Innov. Infrastruct. Solut. 10 (2025) 97, https://doi.org/10.1007/s41062-025-01906-1.
[9] W. Tong, A.M. Memari, State of the art review on hempcrete as a sustainable substitute for traditional construction materials for home building (Article), Buildings 15 (12) (2025) 1988, https://doi.org/10.3390/buildings15121988.
[10] N. Dujardin, T. Salem, V. Feuillet, M. Fois, L. Ibos, C. Poilâne, R. Manuel, Measurement of pore size distribution of building materials by thermal method, Constr. Build. Mater. 240 (2020) 118417, https://doi.org/10.1016/j.conbuildmat.2020.118417.
[11] W.-W. Zhang, Z.-Y. Wei, Y.-Z. Xing, L.-Y. Zhang, Q. Zhang, The effect of pore morphology on thermal insulation properties of thermal barrier coatings, Mater. Chem. Phys. (2024), https://doi.org/10.1016/j.matchemphys.2024.129729.
[12] H. Koshlak, A. Kaczan, The investigation of thermophysical characteristics of porous insulation materials based on Burshtyn TPP Ash, Rocz. Ochr. Środowiska 22 (1) (2020) 537–548.
[13] J. Jiménez-Ruiz, L. Hardion, J.P. Del Monte, B. Vila, M.I. Santín-Montanyá, Monographs on invasive plants in Europe N° 4: Arundo donax L, Bot. Lett. 168 (1) (2021) 131–151, https://doi.org/10.1080/23818107.2020.1864470.
[14] L. HkSuárez, M. Barczewski, P. Kosmela, M.D. Marrero, Z. Ortega, Giant reed (Arundo donax L.) fiber extraction and characterization for its use in polymer composites, J. Nat. Fibers 20 (1) (2022) 1–14, https://doi.org/10.1080/15440478.2022.2131687.
[15] E. Cintura, P. Faria, L. Molari, L. Barbaresi, D. D'Orazio, L. Nunes, Characterization of an Arundo donax-based composite: A solution to improve indoor comfort, Ind. Crops Prod. 204 (2023) 117756, https://doi.org/10.1016/j.indcrop.2023.117756.
[16] R. Leone, L. Lombardo, F. Marchese Ragona, T. Campisi, M. Saeli, Upcycling Arundo donax biomass: A systematic review of applications, materials, and environmental benefits for greener construction, Sustainability 17 (16) (2025) 7402, https://doi.org/10.3390/su17167402.
[17] A. Ayala, J. Ayala, A. Borbón, Optimization of straw-cement-based composites for use as construction materials: A systematic literature review, Int. J. Sustain. Build. Technol. Urban Dev. 16 (2) (2025) 161–192, https://doi.org/10.22712/susb.20250011.

[18] J. Williams, M. Lawrence, P. Walker, The influence of constituents on the properties of the bio-aggregate composite hemp-lime, Constr. Build. Mater. 159 (2018) 9–17, https://doi.org/10.1016/j.conbuildmat.2017.10.109.
[19] Y. Abdellatef, M.A. Khan, A. Khan, M.I. Alam, M. Kavgic, Mechanical, thermal, and moisture buffering properties of novel insulating hemp-lime composite building materials, Materials 13 (21) (2020) 5000, https://doi.org/10.3390/ma13215000.
[20] R. Walker, S. Pavía, Moisture transfer and thermal properties of hemp–lime concretes, Constr. Build. Mater. 64 (2014) 270–276, https://doi.org/10.1016/j.conbuildmat.2014.04.081.
[21] F. Collet, S. Prétot, Thermal conductivity of hemp concretes: Variation with formulation, density and water content, Constr. Build. Mater. 65 (2014) 612–619, https://doi.org/10.1016/j.conbuildmat.2014.05.039.
[22] S.-N. Hong, C.-J. Yu, K.-C. Ri, J.-M. Han, B.-H. Ri, Molecular dynamics study of the effect of moisture and porosity on thermal conductivity of tobermorite 14 Å, arXiv (2020) https://doi.org/10.48550/arXiv.2003.13390.
[23] B. Mazhoud, F. Collet, S. Pretot, J. Chamoin, Hygric and thermal properties of hemp-lime plasters, Build. Environ. 96 (2016) 206–216, https://doi.org/10.1016/j.buildenv.2015.11.013.
[24] L. Ba, A. Trabelsi, T.T. Ngo, P. Pliya, I. El Abbassi, C.S.E. Kane, Thermal performance of bio-based materials for sustainable building insulation: A numerical study, Fibers 13 (5) (2025) 52, https://doi.org/10.3390/fib13050052.
[25] S.T. Pham, Research on the relationship between thermal conductivity and porosity during carbonation of cement materials, Adv. Mater. Res. 1065–1069 (2014) 1838–1841, https://doi.org/10.4028/www.scientific.net/amr.1065-1069.1838.
[26] H. Hachem, I. Mehrez, I. Boumnijel, A. Jemni, D. Mihoubi, Sustainable approach of using Arundo donax leaves reinforced cement mortar/fly bottom ash composites, ACS Omega 8 (13) (2023).
[27] C.A. Schneider, W.S. Rasband, K.W. Eliceiri, NIH Image to ImageJ: 25 years of image analysis, Nat. Methods 9 (7) (2012) 671–675, https://doi.org/10.1038/nmeth.2089.
[28] C. Igathinathane, L.O. Pordesimo, E.P. Columbus, W.D. Batchelor, S.R. Methuku, Shape identification and particle size distribution from basic shape parameters using ImageJ, Comput. Electron. Agric. 63 (2) (2008) 168–182, https://doi.org/10.1016/j.compag.2008.02.007.
[29] European Committee for Standardization. (2015). EN 459–1:2015: Building lime—Part 1: Definitions, specifications and conformity criteria..
[30] E. Aggelakopoulou, A. Bakolas, A. Moropoulou, Lime putty versus hydrated lime powder: Physicochemical and mechanical characteristics of lime-based mortars, Constr. Build. Mater. 225 (2019) 741–751, https://doi.org/10.1016/j.conbuildmat.2019.07.218.
[31] E. Cintura, P. Faria, L. Molari, L. Barbaresi, D. D'Orazio, L. Nunes, Characterization of an Arundo donax-based composite: A solution to improve indoor comfort, Ind. Crops Prod. 208 (2024) 117756, https://doi.org/10.1016/j.indcrop.2023.117756.
[32] M.T. Ferrández-García, C.E. Ferrández-García, T. García-Ortuño, A. Ferrández-García, M. Ferrández-Villena, Experimental evaluation of a new giant reed (Arundo donax L.) composite using citric acid as a natural binder, Agronomy 9 (12) (2019) 882, https://doi.org/10.3390/agronomy9120882.
[33] S. Pochwała, D. Makiola, S. Anweiler, M. Böhm, The heat conductivity properties of hemp–lime composite material used in single-family buildings, Materials 13 (4) (2020) 1011, https://doi.org/10.3390/ma13041011.
[34] M. Kubiś, P. Łapka, Ł. Cieślikiewicz, G. Sahmenko, M. Sinka, D. Bajare, Analysis of the thermal conductivity of a bio-based composite made of hemp shives and a magnesium binder, Energies 15 (15) (2022) 5490, https://doi.org/10.3390/en15155490.
[35] W. Piątkiewicz, P. Narloch, Z. Wólczyńska, J. Mańczak, Effect of hemp shive granulometry on the thermal conductivity of hemp–lime composites, Materials 18 (15) (2025) 3458, https://doi.org/10.3390/ma18153458.
[36] H.H. Humaish, Effect of porosity on thermal conductivity of porous materials, IOP Conference Series Materials Science Engineering 737 (1) (2020) 012185, https://doi.org/10.1088/1757-899X/737/1/012185.
[37] A. Silva, F. Gaspar, A. Bakatovich, Composite materials of rice husk and reed fibers for thermal insulation plates using sodium silicate as a binder, Sustainability 15 (14) (2023) 11273, https://doi.org/10.3390/su151411273.
[38] A. Minoual, S. Mounir, S. Ibn-Elhaj, Y. Maaloufa, H. Sarghini, A. Kabouri, A. Khabbazi, Experimental study of the thermomechanical properties of a new eco-friendly composite material based on clay and reed, J. Compos. Sci. 9 (9) (2025) 469, https://doi.org/10.3390/jcs9090469.
[39] K.B. Kiradjiev, S.A. Halvorsen, R.A. Van Gorder, S.D. Howison, Maxwell-type models for the effective thermal conductivity of a porous material with radiative transfer in the voids, arXiv (2018), https://doi.org/10.48550/arXiv.1812.11696 (Top of Form).
[40] S.R. Latapie, V. Sabathier, A. Abou-Chakra, Bio-based building materials: A prediction of insulating properties for a wide range of agricultural by-products, J. Build. Eng. (2024), https://doi.org/10.1016/j.jobe.2024.108867.
[41] R. Agliata, S. Gianoglio, L. Mollo, Hemp-lime composite for buildings insulation: Material properties and regulatory framework, VITRUVIO Int. J. Archit. Technol. Sustain. 4 (1) (2019) 48, https://doi.org/10.4995/vitruvio-ijats.2019.11771.
[42] M.O. Yusuf, Bond characterization in cementitious material binders using Fourier-transform infrared spectroscopy, Appl. Sci. 13 (5) (2023) 3353, https://doi.org/10.3390/app13053353.
[43] C.N. Checol, Z.B. Sendekie, Effect of alkali treatment on physicochemical and microstructural properties of false banana fiber, Sci. Rep. 15 (2025) 25446, https://doi.org/10.1038/s41598-025-10825-1.
[44] D. Sedan, C. Pagnoux, T. Chotard, A. Smith, V. Gloaguen, Effect of calcium-rich and alkaline solutions on the chemical behaviour of hemp fibres (& others), J. Mater. Sci. 42 (22) (2007) 9336–9342, https://doi.org/10.1007/s10853-007-1903-4.
[45] C. Rodríguez-Navarro, T. Ilić, E. Ruiz-Agudo, K. Elert, Carbonation mechanisms and kinetics of lime-based binders: An overview, Cem. Concr. Res. 172 (2023) 107301, https://doi.org/10.1016/j.cemconres.2023.107301.
[46] S. Benfratello, C. Capitano, G. Peri, G. Rizzo, G. Scaccianoce, G. Sorrentino, Thermal and structural properties of a hemp–lime biocomposite, Constr. Build. Mater. 48 (2013) 745–754, https://doi.org/10.1016/j.conbuildmat.2013.07.096.
[47] M. Ferrandez-Villena, C.E. Ferrandez-Garcia, T. Garcia-Ortuño, A. Ferrandez-Garcia, M.T. Ferrandez-Garcia, The Influence of Processing and Particle Size on Binderless Particleboards Made from Arundo donax L. Rhizome, Polymers 12 (3) (2020) 696, https://doi.org/10.3390/polym12030696.
[48] P. Brzyski, Z. Suchorab, Capillary uptake monitoring in lime-hemp-perlite composite using the time domain reflectometry sensing technique for moisture detection in building composites, Materials 13 (7) (2020) 1677, https://doi.org/10.3390/ma13071677.
[49] E. Cintura, P. Faria, L. Molari, L. Barbaresi, D. D'Orazio, L. Nunes, Characterization of an Arundo donax-based composite: A solution to improve indoor comfort, Ind. Crops Prod. 204 (2023) 117756, https://doi.org/10.1016/j.indcrop.2023.117756.
[50] F. Nicoletti, V. Fiore, R. Tavolanti, T. Scalici, A. Valenza, Effect of various moisture content on the mechanical and viscoelastic properties of giant reed Arundo donax L, Key Eng. Mater. 668 (2015) 317–324, https://doi.org/10.26168/icbbm2015.41.
[51] Z. Pavlík, E. Vejmelková, L. Fiala, R. Černý, Effect of moisture on thermal conductivity of lime-based composites, Int. J. Thermophys. 30 (6) (2009) 1999–2014, https://doi.org/10.1007/s10765-009-0650-y.
[52] R. Malheiro, A. Ansolin, C. Guarnier, J. Fernandes, M.T. Amorim, S.M. Silva, R. Mateus, The potential of the reed as a regenerative building material—Characterisation of its durability, physical, and thermal performances, Energies 14 (14) (2021) 4276, https://doi.org/10.3390/en14144276.
[53] M. Palumbo, A.M. Lacasta, M.P. Giraldo, L. Haurie, E. Correal, Bio-based insulation materials and their hygrothermal performance in a building envelope system (ETICS), Energy Build. 174 (2018) 39–50, https://doi.org/10.1016/j.enbuild.2018.06.042.